Measurement of Accurate Interfluorine Distances in Crystalline Organic Solids: A High-Frequency Magic Angle Spinning NMR Approach

Matthew Fritz[1,2], Jodi Kraus[1,2] Caitlin M. Quinn[1], Glenn P. A. Yap[1], Jochem Struppe[4], Ivan V. Sergeyev[4], Angela M. Gronenborn[2,3,*], Tatyana Polenova[1,2,*]

[1]Department of Chemistry and Biochemistry, University of Delaware, Newark, Delaware 19716, United States; [2]Pittsburgh Center for HIV Protein Interactions, University of Pittsburgh School of Medicine, 1051 Biomedical Science Tower 3, 3501 Fifth Ave., Pittsburgh, PA 15261, United States; [3]Department of Structural Biology, University of Pittsburgh School of Medicine, 3501 Fifth Ave., Pittsburgh, PA 15261, United States; [4]Bruker Biospin Corporation, 15 Fortune Drive, Billerica, MA 01821, United States

***Corresponding authors:** Angela M. Gronenborn, Department of Structural Biology, University of Pittsburgh School of Medicine, 3501 Fifth Ave., Pittsburgh, PA 15260, USA, Tel.: (412) 648-9959; Email: amg100@pitt.edu; Tatyana Polenova, Department of Chemistry and Biochemistry, University of Delaware, Newark, DE, USA, Tel.: (302) 831-1968; Email: tpolenov@udel.edu

ABSTRACT

Long-range interatomic distance restraints are critical for the determination of molecular structures by NMR spectroscopy, both in solution and in the solid state. Fluorine is a powerful NMR probe in a wide variety of contexts, owing to its favorable magnetic properties, ease of incorporation into biological molecules, and ubiquitous use in synthetic organic molecules designed for diverse applications. Due to the large gyromagnetic ratio of the 100% naturally abundant ^{19}F isotope, interfluorine distances as long as 20 Å are accessible in magic angle spinning (MAS) dipolar recoupling experiments. Herein, we present an approach for the determination of accurate interfluorine distances in multi-spin systems, using the finite pulse RFDR (fpRFDR) at high MAS frequencies of 40-60 kHz. We use a series of crystalline "molecular ruler" solids, difluorobenzoic acids and 7F-L-tryptophan, for which the intra- and intermolecular interfluorine distances are known. We describe the optimal experimental conditions for accurate distance determinations, including the choice of a phase cycle, the relative advantages of selective inversion 1D vs. 2D correlation experiments, and the appropriate numerical simulation protocols. A best strategy for the analysis of RFDR exchange curves in organic solids with extended spin interaction networks is presented, which, even in the absence of crystal structures, can be potentially incorporated into NMR structure determination.

INTRODUCTION

In the recent decade, technological progress has been made in the field of biomolecular solid-state MAS NMR, enabling atomic-level structure determination of large biological molecules and assemblies.[1] MAS NMR-based structure determination relies on hundreds of interatomic distance restraints, which are derived from correlation experiments most commonly involving ^{13}C, ^{1}H, and ^{15}N nuclei. The typical distance range accessible through these measurements does not exceed 6-8 Å,[1] which limits the applications to single-domain proteins. Recording longer-range restraints requires introduction of additional probes into the sample, such as paramagnetic spin labels for paramagnetic relaxation enhancement experiments[2] or fluorine labels.[3] The latter approach is rapidly gaining momentum in the solid-state NMR community as the 100% naturally abundant ^{19}F isotope possesses favorable properties, such as its large gyromagnetic ratio. Furthermore, fluorine being absent from naturally occurring biological macromolecules (proteins, nucleic acids, lipids, sugars etc.), is a probe virtually devoid of complications from background signal, and can be readily incorporated into proteins.[4-7] Fluorine-containing functional groups are ubiquitous in man-made organic molecules in diverse contexts: for example, 20-30 % of all pharmaceuticals currently on the market contain one or more fluorine atoms.[8] All these factors have contributed to the rapid growth of ^{19}F solid-state NMR applications,[3, 9-14] aided by the development of modern hardware and, most importantly, probes capable of delivering high MAS frequencies of 40 kHz and above. As recently demonstrated in a number of studies,[3, 10, 12, 15-16] frequencies above 40 kHz are essential for ^{19}F MAS NMR: under these conditions, heteronuclear dipolar and ^{19}F CSA interactions are efficiently averaged out in many of the systems examined to date, alleviating the need for decoupling and permitting measurement of long-range correlations.

Determination of accurate ^{19}F-^{19}F distances from correlation experiments requires robust dipolar recoupling sequences. An ideal sequence has a high scaling factor, is insensitive with respect to the isotropic and anisotropic chemical shifts as well as B_1-field inhomogeneity and has radio frequency (rf) power requirements that are easily attainable with the available hardware. Many dipolar recoupling sequences exist, and each is suitable for a particular range of experimental conditions. For example, sequences where the required rf power scales with the spinning rate may not be applicable for high MAS frequencies (> 40 kHz). Homonuclear recoupling experiments of the general C-symmetry class CN_2^1, including their supercycled versions do not compensate well enough for interference from CSA and experimental imperfections to be reliable over long recoupling times.[17] Furthermore, because of their rf amplitude requirements, applications have been limited to MAS rates of 40 kHz and below.[18] Second-order methods, such as R-symmetry driven spin diffusion (CORD, PARIS, PARIS-xy, and

SHANGHAI) for fluorine require specialized hardware since ^{1}H irradiation is used to drive spin diffusion. Moreover, the efficiency of these experiments drops dramatically as the MAS frequency increases.[19-22]

Radio frequency driven recoupling (RFDR) is a robust method for dipolar recoupling.[23] A seminal study from Gilchrist and McDermott[24] demonstrated that accurate interfluorine distances can be recorded, in the regime of a single spin pair, using ^{19}F-^{19}F RFDR recoupling when MAS frequencies are as low as 6 kHz. We and others exploited ^{19}F-^{19}F RFDR for correlation spectroscopy at MAS frequencies of up to 60 kHz. [3, 10, 15] Yet, a systematic investigation into the experimental requirements and the validation of the distances derived via RFDR experiments at high MAS frequencies and in dipolar coupled multi-spin systems has been lacking.

RFDR is easy to implement, the sequence is forgiving of rf mismatch and has modest rf power requirements. Furthermore, at high MAS frequencies, ^{19}F-^{19}F RFDR experiments can be performed without heteronuclear decoupling.[3, 15] It is also worth noting that the basic sequence τ-180_0-τ satisfies the requirements to be considered an RN-symmetry element and RFDR sequences can been modified using symmetry principles, thereby maximizing the efficiency of the recoupled dipolar term while eliminating other unwanted spin interactions.[25] Specifically, the XY4 phase cycled RFDR sequence corresponds to the $[R4_4^{-1}]_{45}$ symmetry. According to the selection rules for $[R4_4^{-1}]_{45}$, first-order CSA and heteronuclear dipolar couplings are forbidden, while homonuclear dipolar couplings and the isotropic J coupling are reintroduced. Second-order terms containing CSA and heteronuclear dipolar couplings scale with the inverse of the spinning frequency.[26] Consequently, the latter are reduced at fast spinning conditions (MAS frequencies of > 40 kHz) and can be further attenuated with appropriate phase cycling.[27] At MAS frequencies of 60 kHz and higher, the rotor periods become very short: for example, τ_r=16.67 μs at ω_r=60 kHz. In this regime, the finite pulse limit is reached and the recoupling pulse comprises a significant fraction of the rotor period, the so-called finite-pulse RFDR (fpRFDR) condition.[28] With its Hamiltonian being proportional to the static dipolar Hamiltonian, fpRFDR affords flexibility with regard to chemical shift difference (i.e., recoupling is efficient even when the isotropic chemical shift difference is small) and rf field requirements. This is important because fluorinated compounds with the same basic chemical scaffold (aromatic CF groups or CF_3 moieties at different positions in the aromatic ring) exhibit limited chemical shift dispersion, a disadvantage in conventional RFDR, whereby sites with small isotropic chemical shift differences cannot be efficiently recoupled, because the Hamiltonian is proportional to the flip-flop term.[28]

The goal of the work presented here is to provide strategies for the successful application of fpRFDR to homonuclear ^{19}F recoupling at high MAS frequencies of 40-60 kHz for accurate

interfluorine distance extraction in organic crystalline solids with extended spin interaction networks. We examine the performance of fpRFDR in a series of microcrystalline “molecular rulers” displayed in Figure 1 A-D: difluorobenzoic acids and 7F-L-tryptophan (7F-L-Trp), for which interfluorine intra- and intermolecular distances are known. This series was chosen since the ^{19}F chemical shifts in these molecules cover a large range (~100 ppm) and they serve as mimics of fluoro-containing functional groups in proteins. We show that assignments of ^{19}F chemical shifts can be readily achieved using density functional theory (DFT) calculations. We discuss the advantages and limitations of two different implementations of the fpRFDR sequence: the 2D fpRFDR correlation experiment and its 1D version, where selective inversion is followed by RFDR mixing, as originally introduced by McDermott and coworkers.[24] We demonstrate that the 1D experiment, with initial selective magnetization inversion for the spin of interest, using the “delays alternating with nutation for tailored excitation” (DANTE) sequence,[29] followed by fpRFDR mixing, is advantageous for these model compounds. This experiment permits recording detailed RFDR exchange curves in a fraction of the time required for a corresponding series of 2D experiments are used. We show that the choice of the phase cycling scheme is dictated by the nature of the functional groups to be recoupled. When fine sampling of the initial magnetization exchange profile is required, the XY16 phase cycle is optimal while the with $(XY8)4^1$ phase cycle is preferable for long mixing times. We also assessed the requirements for numerical simulations of the RFDR magnetization exchange in these multi-spin systems and show that accurate interfluorine distances can be inferred from these recoupling experiments, even without the *a priori* knowledge of the crystal structures. We envision that our approach will be broadly applicable to organic and biological systems, including large biological assemblies.

MATERIALS AND METHODS

Fluorinated model compounds

2,3-difluoro-benzoic acid (Lot No: GBFA010899), 2,4-difluoro-benzoic acid (Lot No: 10060297), and 2,5-difluoro-benzoic acid (Lot No: Y20A033) were purchased from Alfa-Aesar. 7F-L-Trp was purchased from Amatec Chemical Co. Ltd (Hong Kong) (Lot No: 12551). All the compounds with the exception of 2,5-dilfuorobenzoic acid and 7-L-Trp were used without further purification.

Crystallization of 7F-L-Trp and 2,5-difluorobenzoic acid and crystal structure determination

7F-L-Trp was recrystallized from a 30% water/isopropanol mixture. For 2,5-difluorobenzoic acid, crystals were grown as previously described using by liquid-liquid diffusion in a binary solvent system of methanol and hexane.[30] Crystals suitable for X-ray diffraction were grown at ambient temperature.

Crystal structure determination and X-ray structural analysis for 7F-L-Trp and 2,5-difluorobenzoic acid

Crystals were mounted using viscous oil onto a plastic mesh and cooled to the data collection temperatures. Data were collected on a Bruker-AXS APEX II DUO CCD diffractometer with Cu-Kα radiation (λ = 1.54178 Å) focused with Goebel mirrors or with graphite monochromated Mo-Kα radiation (λ = 0.71073 Å). Unit cell parameters were obtained from 36 to 48 data frames, 0.5º ω, from different sections of the Ewald sphere.[31] Although the structure of 2,5-fluorobenzoic acid has been previously reported,[30] we attempted to get a higher precision structure by using higher resolution data (0.6 Å) at lower temperature (100 K). The systematic absences in the diffraction data for 7F-L-Trp are consistent with $P2_1$ and $P2_1/m$; however, the absence of a molecular mirror plane, the occupancy and the chirality of the compound were consistent only with $P2_1$. The Flack parameter refined to virtually nil, indicating that the correct handedness has been determined. The data were treated with multi-scan absorption corrections.[31] The structures were solved using intrinsic phasing methods[32] and refined with full-matrix, least-squares procedures on F^2.[33] Non-hydrogen atoms were refined with anisotropic displacement parameters. The compound molecule for 2,5-fluorobenzoic acid was found disordered in two positions with a refined site occupancy of 0.827/0.173. For 7F-L-Trp, H-atoms were located from the difference map and refined with isotropic parameters. For 2,5-fluorobenzoic acid, both disordered carboxylic H-atoms were initially located from the difference map with the major component H-atom position allowed to refine. All

other H-atoms were constrained in idealized positions with isotropic parameters based on their attached atoms. Atomic scattering factors are contained in the SHELXTL program library.[33] The structure has been deposited at the Cambridge Structural Database under depositary numbers CCDC 1953345 (7F-L-Trp) and 1953545 (2,5-difluorobenzoic acid). Detailed information on each X-ray crystal structure corresponding refinement statistics can be found in the Supporting Information.

^{19}F MAS NMR experiments.

^{19}F MAS NMR experiments on 2,3-difluorobenzoic acid, 2,4-difluorobenzoic acid, 2,5-difluorobenzoic acid, and 7F-L-Trp crystals were carried out at 14.1 T, on a Magnex narrow-bore magnet interfaced with a Bruker AVIII HD spectrometer, and outfitted with a 1.3 mm Bruker HCN MAS probe. The H channel was tuned to the ^{19}F Larmor frequency of 564.278 MHz. 3.4 mg of 2,3-difluorobenzoic acid, 3.8 mg of 2,4-difluorobenzoic acid, 3.5 mg of 2,5-difluorobenzoic acid, and 3.2 mg of crystalline 7F-L-Trp were packed into 1.3 mm Bruker rotors. ^{19}F MAS NMR spectra were collected at MAS frequency of 60 kHz for all compounds and an additional set of spectra for 7F-L-Trp crystals was acquired at 10 kHz. The frequencies were controlled to within ±5 Hz by a Bruker MAS controller. The actual sample temperature was calibrated using KBr as a temperature sensor and was maintained at 22±1 °C throughout the experiments, using a Bruker temperature controller. The typical ^{19}F 90° pulse length was 3 μs. The recycle delays were 120 s. No ^{1}H decoupling was applied in any of the experiments. The spin-lattice relaxation times T_1 were recorded with the saturation-recovery sequence. ^{19}F chemical shifts were indirectly referenced to the adamantane-referenced ^{13}C chemical shifts.[34] 5-^{19}F-DL-Trp powder was used as a secondary reference standard, -44.6 ppm at 290 K.

For 2D fpRFDR experiments, the pulse sequence shown in Figure 2A was used. The data were typically acquired as 3072×16 complex matrices, with 8 transients added for each FID. States-TPPI phase sensitive detection was used in the indirect dimension.[35] The RFDR buildup curves were acquired with mixing times of 0.8, 1.06, 1.33, 1.6, 2.13, 3.2, 4.26, 8, 12, 16, and 32.0 ms.

The pulse sequence for the 1D DANTE-RFDR experiment is shown in Figure 2B. The pulse length for the DANTE selective inversion pulses was 0.1 μs, and m was set to 1 or 2. For 7F-L-Trp, the dipolar exchange curves were acquired with the fpRFDR mixing times incremented from 0.533 ms to 32.0 ms in steps of 0.533 ms. For 2,4-difluorobenzoic acid and 2,5-difluorobenzoic acid the fpRFDR mixing times in the corresponding experiments were 0.533, 1.066, 1.599, 2.132,

2.665, 3.198, 3.731, 4.264, 4.797, 5.330, 5.863, 6.396, 6.929, 7.462, 7.995, 8.528, 10.66, 12.792, 14.924, 17.056, 21.320, 25.584, 29.848, and 32.000 ms.

The 2D spectra were processed in TopSpin with 500 Hz exponential line broadening and forward linear prediction, and analyzed in NMRFAM-Sparky.[36] Error bars were defined according to the following equation:

$$\sigma = \sqrt{\left(\frac{1}{SNR_{AB}}\right) + \left(\frac{1}{SNR_{AA}}\right) + \left(\frac{1}{SNR_{BB}}\right)}$$

Where SNR is the signal-to-noise ratio of a cross peak of interest.

The 1D spectra were processed with either NMRPipe[37] or MNova, and absolute intensities were extracted. Error bars in the 1D DANTE-RFDR are defined as the standard deviation of the noise over a 10 ppm region devoid of signal. Both parameters were multiplied by the normalized intensity.

Density functional theory calculations

All DFT calculations were performed using the Gaussian09 program.[38] All-atom geometry optimizations and NMR shielding calculations were performed using the M06 density functional and cc-pVTZ basis set in conjunction with the SMD solvation model.[39-40] The ^{19}F chemical shifts were referenced by converting absolute magnetic shieldings, σ_i, to chemical shifts using the relation $\delta_i = \sigma_{ref} - \sigma_i$, with the value of σ_{ref} determined by linear regression between calculated and experimental shifts.[41] ^{19}F chemical shift tensor parameters were defined according to the Haeberlen-Mehring-Spiess convention. The isotropic chemical shift δ_{iso}, the reduced anisotropy δ_σ, and the asymmetry parameter η, are related to the principal components of the chemical shift tensor, δ_{ii} (i = 1, 2 or 3) according to $|\delta_{11} - \delta_{iso}| \geq |\delta_{33} - \delta_{iso}| \geq |\delta_{22} - \delta_{iso}|$, $\delta_{iso} = {}^{1}/_{3}\,(\delta_{11} + \delta_{22} + \delta_{33})$, $\delta_\sigma = \delta_{11} - \delta_{iso}$, and $\eta = {}^{(\delta_{22} - \delta_{33})}/_{(\delta_{11} - \delta_{iso})}$. Details of the calibration sets and coordinates of the molecular rulers are given in the Supporting Information.

Numerical simulations

Longitudinal magnetization exchange as a function of mixing time was simulated using SIMPSON version 1.1.2[42] in a MacOS environment. Multispin simulations used SIMPSON versions 3.0.0 and 4.0.0 in a Linux and in NMRbox environments, respectively. For the simulation of 2D RFDR, the magnetization transfer from I_{1z} to I_{2z} was followed, whereas for DANTE-RFDR I_{2z} to I_{2z}-I_{1z} was followed.

For buildup curves and multi-spin simulations, a powder average was generated according to the ZCW[43] scheme with 615 pairs of {α, β} angles and 13 γ-angles. To produce a powder average for the phase cycle analysis, 168 pairs of {α, β} angles were generated according to the REPULSION algorithm[44] and 13 γ-angles (resulting in a total of 2,184 angle triplets) were used for all simulations. NMR parameters in the experiment matched those used during the simulation routine. The simulated intensities were scaled such that the maximum intensity matched the experimental maximum. The corresponding SIMPSON scripts are given in the Supporting Information.

A grid of 3000 five-spin systems was generated, where the intramolecular ^{19}F-^{19}F distance was varied from 4.6 Å to 5.6 Å in 0.2-Å steps. A third (truncating) spin was present at a distance of 2.8 to 3.6 Å, incremented in 0.2-Å steps. A fourth and a fifth spin were placed each at a distance of 4.2 Å to 6.0 Å, incremented in 0.2-Å steps. For each of these spin systems, DANTE-RFDR $(XY8)4^1$ magnetization exchange curves were simulated in SIMPSON using the same protocol outlined above for the multi-spin simulations. The corresponding SIMPSON and Python scripts are given in the Supporting Information.

RESULTS AND DISCUSSION

^{19}F MAS NMR spectra of molecular rulers

Molecules used as distance rulers in this study comprise a series of benzoic acids with fluorine substitutions in the 2,3- 2,4- and 2,5- positions on the benzyl ring and crystalline L-tryptophan with a fluorine substitution in the 7-position of the indole ring. The positioning of two neighboring molecules in the crystallographic unit cells as well as the ^{19}F MAS NMR spectra are shown in Figure 1 A-D. The individual fluorine resonances are well resolved and all chemical shifts and spin-lattice relaxation times are summarized in Table 1. The chemical shift differences for the two fluorine resonances for an individual difluorobenzene is ca. 2.5-4 ppm, and the 2-fluorine resonances in the different 2,3, 2,4 and 2,5-difluorobenzene molecules vary from -27 to -60.4 ppm. For 2,5-difluorobenzoic acid crystals, the resonances are broadened, which we attribute to the presence of positional disorder, see below and Supporting Information. Interestingly, in the 7F-L-Trp ^{19}F MAS NMR spectrum, two distinct resonances at -53.1 and -56.4 ppm are observed, corresponding to the two crystallographically inequivalent fluorine atoms in the unit cell, separated by 3 Å (Figure 1D and in Tables S1-S4 of the Supporting Information). These results illustrate the exquisite sensitivity of ^{19}F chemical shifts to the local environment around the fluorine atom.

^{19}F chemical shift assignment by DFT calculations

One challenge in the application of ^{19}F MAS NMR is the assignment of chemical shifts. Often simple chemical knowledge is insufficient to derive the assignments[45] as exemplified by the chemical shifts of the 2F- atom in the different difluoro-substituted benzoic acids used in this study (Figure 1A-C). One approach for assigning the resonances would be to measure ^{19}F-^{13}C correlations, but this is typically not feasible without specialized probe hardware. Furthermore, in natural abundance materials, such as pharmaceuticals, these experiments are often time consuming. Two recent studies reported that qualitative assignments of the ^{19}F isotropic chemical shifts of small molecules could be straightforward by DFT calculations.[45-46] Accurate prediction of ^{19}F chemical shift tensors is currently an active area of research and such studies are computationally very demanding.[15] However, deriving assignments on the basis of chemical shift trends, calculated for a series of chemically similar compounds appears to be computationally feasible and possibly of predictive value. This is the approach we undertook here. Specifically, we first ascertained that the trends in magnetic shieldings could be accurately reproduced in DFT calculations for a subset of fifteen fluorinated aromatic molecules exhibiting twenty-two unique shifts (Figure S1 of the Supporting Information). We then used these trends to assign the chemical

shifts for the molecular ruler molecules under investigation. As shown in Figure S2 of the Supporting Information, exceptionally good agreement is reached between experiment and theory, with the slope of the correlation between experimental chemical shifts and the DFT calculated shieldings of -1.03 and R^2 of 0.99. Using this calibration set, we calculated the magnetic shieldings for the model difluoro-substituted benzoic acids and 7F-L-Trp molecular rulers under investigation and used these values to assign their corresponding chemical shifts. These are listed in Table 1.

Most gratifyingly, the DFT calculations yielded non-negligible chemical shift differences for the two crystallographically inequivalent fluorine atoms of the neighboring molecules in 7F-L-Trp, even using the minimal representation of the unit cell. Furthermore, the relative magnitudes of the CSA tensor (to be reported elsewhere) are captured by the calculations. While the current DFT analysis does not allow for quantitative predictions of absolute CSA tensors, it permits assignment of relative shifts for resonances exhibiting small differences in isotropic shifts.

Selection of RFDR phase cycle

Several phase cycling schemes are commonly used in RFDR experiments.[25, 47] Phase cycling can remove deleterious CSA effects, differences in resonance frequency, rf inhomogeneity, and heteronuclear dipolar couplings. Additional advantages are imparted by MAS frequencies of 40-60 kHz. Fast MAS efficiently removes CSA and heteronuclear couplings, and satisfying the finite pulse limit permits efficient recoupling of sites with close resonance frequencies (see Figure S3 of the Supporting Information). Increased tolerance to experimental imperfections is an added advantage. Most supercycles, such as XY16, compensate well for rf field inhomogeneity, and even the XY4 cycle appears to be sufficient in the strong coupling limit and for short mixing times.[25]

In this study, we compared two phase cycles, XY16 and $(XY8)4^1$. Both are supercycles of XY8: XY16 is an inversion cycle whereas $(XY8)4^1$ is a global supercycle with four repetitions of XY8, each with an overall 90-degree phase shift. The XY8 phase cycle removes second-order cross terms that are proportional to zero-quantum spin operators. Second-order cross terms, such as cross-terms between the ^{19}F CSA and homonuclear dipolar coupling as well as between the ^{19}F CSAs of the interacting spins, can obstruct recoupling, especially at long mixing times. Figure 3A displays the buildup curves for both phase cycles recorded in 2D RFDR experiments, illustrating that for both phase cycles the initial buildup rates and the plateau magnitudes are identical. However, beyond 20 ms complete loss of magnetization is observed for the XY16 phase cycle. The numerical simulations of the RFDR buildup curves (Figure 3B) reveal that the $(XY8)4^1$ cycle reduces CSA interference, compared to XY16, most notably for longer recoupling times.

While intensity losses at mixing times beyond 5 ms are expected in the presence of CSA for both phase cycles, the average intensity loss throughout the curve is 38% for XY16 and only 21 % for $(XY8)4^1$. These results are also borne out experimentally: nearly complete magnetization loss was observed for all compounds at 32.0 ms mixing time with the XY16 phase cycle, while intense resonances are still present when the $(XY8)4^1$ cycle was used (Figure S4 of the Supporting Information).

Figure 3C depicts the dependence of RFDR signal on the difference between the isotropic chemical shifts of the recoupled resonances and the reduced anisotropy of the detected spin, at a MAS frequency of 60 kHz, RFDR mixing time of 6.4 ms and assuming a ^{19}F-^{19}F dipolar coupling constant of 1602.12 Hz, corresponding to an interfluorine distance of 4.05 Å. The corresponding plots for the MAS frequencies of 40 and 80 kHz are provided in Figure S4 of the Supporting Information. As can be appreciated, at MAS frequencies of 40 and 60 kHz, the recoupling efficiencies are comparable for both phase cycles and no noticeable intensity drop is observed until the CSA exceeds the MAS frequency. These simulations also suggest that intensity should be present at long mixing times with XY16. However, we did not observe this experimentally, possibly due to intensity losses associated with zero-quantum relaxation.[24, 48] Interestingly, at 80 kHz, the simulations suggest very efficient recoupling with the $(XY8)4^1$ cycle over a broad range of conditions, while for XY16 no signal intensity is present at all. Taken together, both the experimental and the numerical simulation results indicate that with $(XY8)4^1$ the magnetization can be retained at long RFDR mixing times. For the compounds under investigation, the mixing time of 32.0 ms is much longer than required for accurate distance measurements. Nonetheless, in cases where interfluorine distances are much longer or where slower MAS frequencies are required, $(XY8)4^1$ would be the phase cycle of choice, to prevent the loss of magnetization due to interference from CSA.

Interfluorine distances in difluorobenzoic acids and 7F-L-Trp

In order to derive interfluorine distances for the current set of molecules, RFDR spectra were acquired in 2D fpRFDR and 1D DANTE-fpRFDR experiments as a function of RFDR mixing time. In the latter, a selective inversion pulse train was applied prior to the RFDR mixing period. As demonstrated in early studies, by replacing a hard pulse with a selective inversion pulse sequence, such as DANTE, RFDR exchange curves can be recorded in a series of one-dimensional experiments.[24] The main advantages are the time savings associated with the reduced dimensionality, which as a consequence allows for denser sampling of time points of the magnetization exchange/buildup profile. This strategy was particularly beneficial here, given only

two well resolved resonances in all spectra and the long T_1 value of 7F-L-Trp (215 s). In practice, this translates into an overnight experiment for the acquisition of 60 time points in a series of 1D DANTE-RFDR spectra, compared to several days for the acquisition of 10 time points in a series of 2D RFDR data sets.

While prior reports on interfluorine distance measurements employed systems for which a single spin pair approximation was valid,[10, 24] we deliberately chose to work in the multi-spin regime. This regime is ubiquitous in crystalline organic solids with dense networks of coupled spins and may also be encountered in proteins when multiple residues are fluorinated. Specifically, the difluorobenzoic acids under investigation form hydrogen bonded dimers in the crystal, resulting in intermolecular dipolar couplings of the same order of magnitude as or even stronger than intramolecular couplings. The associated distances are illustrated in Figure 1 and 4.

Figure 4A shows simulated RFDR signal buildups for a model system comprised of four dipolar coupled spins, with the intramolecular F-F distance of 4.2 Å and intermolecular distances between 2.9 and 4.2 Å. This is a realistic scenario for the molecules under investigation here. For comparison, using only the intramolecular distances in single spin pair approximations, buildup profiles were also calculated and are shown in black. These curves exhibit the expected features: the signal builds up within the first 3 ms and after 9 ms oscillates around a plateau intensity of 0.8. If a third spin, at a distance of 2.9 Å, is added in the simulation, the magenta buildup profile is obtained. In this case, the initial rate is faster than in the two-spin case, given the shorter distance of the third spin. Including a fourth spin, at a distance of 3.9 Å, the cyan buildup profile is obtained. Two distinct features are worth pointing out: first, the initial buildup is biphasic, with two effective rise times, qualitatively corresponding to the two shortest distances. Second, the oscillations are greatly dampened after the maximum intensity is reached and essentially no intensity loss occurs over 16 ms of mixing. These buildup profiles are clearly different from the curves for two spins at distances of 3.9 Å and 4.2 Å (Figure S5 of the Supporting Information). Finally, if a fourth spin separated by a much longer distance, 7 Å, is added in the simulations, its presence does not affect the buildup profile (Figure S6 of the Supporting Information). This is a direct consequence of the well-known phenomenon of dipolar truncation.[49] Overall, these simulations reveal two limiting scenarios: i) if one of the spins in the coupled networks is at a much longer distance with respect to the spin of interest, compared to other spins within the network, its effect on the corresponding RFDR buildup is negligible; ii) if all spins in the network are at similar distances to the spin of interest, they all contribute to the RFDR buildup profile and have to be treated by multi-spin simulations.

With the above considerations in mind, we inspected our experimental results. Of the molecules under investigation, 2,3-difluorobenzoic acid is the only compound where the intramolecular ^{19}F-^{19}F distance is shorter than any of the intermolecular contacts. The experimental 2D-RFDR buildup curve is shown in Figure 4B, and the geometry of the neighboring fluorine atoms in Figure 4C. The initial buildup rate is consistent with an intramolecular distance of 2.6 Å, since the maximum intensity is reached at 1.0 ms. Interestingly, no pronounced signal decay was observed experimentally even at an RFDR mixing time of 16 ms. This suggests that multi-spin effects have to be considered. Indeed, the inspection of the X-ray crystal structure reveals that, in addition to a short intramolecular F-F distance, 4 other intermolecular, F-F distances, ranging between 3.2 and 5.7 Å, to neighboring molecules are present. The resulting additional couplings dominate the buildup curve at the mixing times beyond 1.0 ms, the point where the signal due to intramolecular coupling begins to decay. The best agreement with the experiment is observed in a six-spin simulation.

As demonstrated in a previous study, at MAS frequencies of 40 kHz and above, the effect of ^{19}F CSA is small and can be neglected for distance measurements by RFDR.[10] We nevertheless examined the possible influence of ^{19}F CSA on the RFDR buildup curves for 2,3-difluorobenzoic acid. ^{19}F CSA tensor parameters predicted by DFT calculations were employed, as experimental measurements are currently out of reach. We note that the contribution of the CSA to the initial RFDR signal buildup is negligible (Figure S7 of the Supporting Information) and multi-spin couplings attenuate the interference from the CSA even further. Therefore, we can neglect the influence of CSA for the remainder of the current study.

In Figure 4D-F, the results of DANTE-RFDR and 2D RFDR experiments, together with the interfluorine coupling network are shown for 7F-L-Trp. In the crystal form we used for our measurements, two crystallographically inequivalent fluorine atoms per unit cell give rise to two resonances with unique ^{19}F isotropic chemical shifts in the MAS NMR spectra. The interfluorine distances between each crystallographically unique fluorine and its neighbors range from 3.0 Å to 8.7 Å, with the most frequently observed distance at 4.7 Å. Consistent with these distances, the experimental RFDR magnetization exchange is fast. For the DANTE-RFDR curve, the shortest distance of 3.0 Å is sufficient to reproduce the experimental initial magnetization exchange profile, while for the 2D RFDR, the signal intensity reaches the first and second maxima at 1.6 and 4.3 ms, respectively, indicating the contribution of multiple spins to the buildup. Indeed, the best fit between the simulated and experimental 2D RFDR buildup curve requires the summation of the two-spin and five-spin networks. This seems reasonable, since contributions from distances longer than 3.0 Å have to be taken into account.

Figure 4G-I shows the experimental DANTE-RFDR and 2D-RFDR curves, together with the interfluorine coupling network for 2,4-dilfuorobenzoic acid. The experimental curves could be accurately simulated using a four-spin system, comprising an intramolecular pair of distances of 3.5 Å and intermolecular distances of 3.7 Å. The intermolecular couplings contribute additional signal intensity at longer mixing times, a distinct feature of multi-spin effects. Simulated magnetization exchange curves for two-, three-, and four-spin systems (Figure S7 of the Supporting Information) illustrate that at least four spins are required to reach agreement with experiment.

In Figure 4J-L, the results of DANTE-RFDR and 2D RFDR experiments are shown for 2,5-difluorobenzoic acid, together with the interfluorine coupling network. In the crystal structure of 2,5-difluorobenzoic acid, the fluorine atoms in positions 2 and 5 show occupancies of 0.810:0.190 (F2a and F2b) and 0.790:0.210 (F5a and F5b), reflecting alternative orientations in the crystal lattice. As a result, two types of extended lateral interactions in the crystal have to be considered (Figure 4L). The resulting interaction networks are indistinguishable by NMR, since the chemical shifts for the positional isomers are identical, and only two resonances, one for each type of fluorine substitution, are present in the spectra, although the lines for each are about twice as broad as for other compounds under investigation. To account for the positional disorder, for each isomer we constructed clusters of four molecules and five spins, as illustrated in Figure 4L. For these clusters, we ran five simulations, systematically interchanging the states with the higher and the lower occupancy for each of the spins, accounting for their relative populations in the crystal lattice. As shown in Figure 4J,K, the simulated RFDR exchange curves (black lines) are in very good agreement with the experimental data points, while, in contrast, the simulation for a single spin pair (blue lines) exhibits poor agreement with the experimental points.

Analysis of RFDR exchange curves without a priori knowledge of distances between the coupled spins

As demonstrated above, the ^{19}F RFDR experiments at a MAS frequency of 60 kHz are well suited for determining accurate interfluorine distances in crystalline materials. The sequence is forgiving with respect to the applied rf field requirements and performs well in the absence of heteronuclear decoupling. Even though the RFDR magnetization exchange profiles are affected by the presence of multiple intra- and/or inter-molecular ^{19}F-^{19}F dipolar couplings, the exchange curves can be readily calculated when the crystal structure is available. As discussed below, accurate distances can also be extracted in the absence of a X-ray crystal structure, rendering simulations of RFDR curves a useful approach for characterizing fluorinated solids.

In cases where the distances are not known, estimates for intramolecular interfluorine distances can be used as starting values for the simulation of RFDR magnetization exchange profiles. Since the initial rate of the magnetization exchange is dominated by the shortest distance, this rate will provide an immediate estimate for the shortest distance. If the magnetization builds up at rates consistent with the estimated intramolecular distance, this closest intramolecular dipolar interaction is dominant. If the initial magnetization builds up at a faster rate than estimated, one or more other dipolar coupled fluorine atoms contribute to the magnetization exchange. In the simplest case, the magnetization exchange is affected by a single coupling, corresponding to the shortest interfluorine distance. In complex cases, the initial magnetization buildup rate is faster than estimated and the intensity maximum is reached at mixing times longer than estimated for a single spin pair, i.e. multiple spins contribute to the buildup. This case is illustrated in Figure 4A for a four-spin system. To estimate the distances between spins in the multi-spin RFDR curve, a series of two-spin simulations is carried out in which the distances are systematically varied (see Figure S5 of the Supporting Information as an example). Once the distance ranges are known for the two-spin simulation, additional simulations for three, four, and five-spins can be performed. From the results presented here, it appears that five-spin systems should be sufficient to reproduce the buildup curves for many organic crystals with extensive coupling networks.

We tested the above assertion on 2,5-difluorobenzoic acid, the most complicated molecule due to the positional disorder. We generated a grid of 3000 five-spin systems. In these, the intramolecular ^{19}F-^{19}F distance was varied from 4.6 Å to 5.6 Å in 0.2-Å steps; a third (truncating) spin was present at a distance of 2.8 to 3.6 Å, also incremented in 0.2-Å steps; a fourth and a fifth spin were each at a distance ranging of 4.2 Å to 6.0 Å, varied in 0.2-Å steps. This array of distances is representative of the series of difluorobenzoic acids under investigation and generally of organic crystals of fluorinated molecules of similar size. Using the above five-spin system distance grid, we simulated the corresponding ^{19}F RFDR exchange curves and best fit of the simulated and the experimental RFDR curves permitted extraction of distances of 5.6 Å (intramolecular), 3.6 Å (to the third spin), 6.0 Å (to the fourth spin) and 4.2 Å (to the fifth spin). These are in remarkably good agreement with those extracted from the X-ray structure, which has a 5.4 Å (intramolecular) distance for the major-occupancy site, 3.5 Å (to the third spin), 5.9 Å (to the fourth spin), and 5.1 Å (to the fifth spin). As can be appreciated from Figure 4J, the best-fit (smallest-RMSD) simulation from the synthetically generated five-spin grid (magenta line) closely agrees with the experiment. This result is gratifying and indicates that, multi-spin interaction networks can be determined *de novo* from the RFDR exchange curves. We envision that the distance information extracted from the ^{19}F-^{19}F RFDR magnetization exchange curves

can be used in conjunction with other information, such as ^{19}F, ^{13}C, and ^{1}H chemical shifts and other types of correlation experiments, to determine structures of fluorinated solids, as has been successfully done for a number of other systems in an “NMR crystallography” approach.[50]

We also note that fluorinated molecules can be diluted with non-fluorinated analogs for the removal of intermolecular effects, as has been shown in previous studies.[10, 51] However, this requires crystallization of the mixture and solution of the crystal structure of such mixed materials, which may not be straightforward. Furthermore, for pharmaceutical preparations, the non-fluorinated molecule may not crystallize in the same crystal form. Therefore, the approach presented here is the most general, as it leverages the strengths of high-speed ^{19}F MAS NMR where contributions to the homonuclear dipolar exchange from other interactions (CSA, heteronuclear dipolar and scalar) are negligible, as well as numerical simulations for the interpretation of exchange curves in the presence of dense networks of dipolar couplings.

Furthermore, for biological molecules and assemblies, where the unit cells are much larger and fluorine sites are sparse, complications from multi-spin effects will be rare.

CONCLUSIONS

A robust approach for the extraction of interfluorine distances in organic and biological solids by MAS NMR is presented. At fast spinning frequencies of 40 – 60 kHz, efficient recoupling of ^{19}F-^{19}F dipolar interaction is accomplished by the fpRFDR sequence, even for sites with small chemical shift differences, and where the effects of other spin interactions on magnetization exchange are negligible. For compounds with known X-ray crystal structures, accurate interfluorine distances are obtained by numerical simulations of RFDR magnetization exchange curves, taking into account multiple dipolar couplings that contribute to the magnetization exchange into account. For compounds with unknown structures, we present a strategy for the analysis of experimental RFDR data which permits assessment of the presence and relative contribution of multi-spin systems. The approach presented here is broadly applicable to organic and biological molecules and is envisioned to be particularly useful for structural analysis of solid fluorine-containing pharmaceuticals, large biological assemblies, and complexes thereof.

SUPPORTING INFORMATION AVAILABLE

Chemical structures of fluorinated aromatic compounds used for calibrating ^{19}F chemical shifts in the DFT calculations; correlation between experimental solution NMR and calculated ^{19}F isotropic chemical shifts for the fluorinated aromatic compounds under investigation; simulated RFDR signal intensities and buildup/exchange curves as a function of various experimental parameters and presence of multi-spin effects; for recrystallized 7F-L-Trp and 2,5-difluorobenzoic acid– i) X-ray structure determination protocols; ii) crystal data and structure refinement parameters; iii) atomic coordinates and equivalent isotropic displacement parameters; iv) bond lengths and bond angles; v) anisotropic displacement parameters; vi) hydrogen coordinates and isotropic displacement parameters; experimental and calculated ^{19}F NMR chemical shifts of fluorinated aromatic compounds used as a calibration set for DFT calculations; SIMPSON and Python simulations and analysis scripts; Gaussian input files. This information can be found on the internet at http://pubs.acs.org.

ACKNOWLEDGMENTS

This work was supported by the National Science Foundation (NSF Grant CHE-1708773 to AMG and TP) and by the National Institutes of Health (NIH Grant P50AI150481, Technology Development Project 2) and is a contribution from the Pittsburgh Center for HIV Protein Interactions. JK is supported by the National Science Foundation Graduate Research Fellowship Program (#1247394). We acknowledge the support and of the National Institutes of Health (NIH Grant P30GM110758) for the support of core instrumentation infrastructure at the University of Delaware. This study made use of NMRbox: National Center for Biomolecular NMR Data Processing and Analysis, a Biomedical Technology Research Resource (BTRR), which is supported by NIH grant P41GM111135 (NIGMS). GY thanks Maxwell I. Martin for work on the 2,5-fluorobenzoic acid structure.

AUTHOR CONTRIBUTIONS

T.P. and A.M.G. conceived the project and guided the work. M.P.F. prepared the samples, performed NMR experiments, analyzed the experimental data, and conducted the DFT calculations and numerical simulations. J.K. crystallized the sample of 7F-L-Trp, contributed to the NMR experiments and data analysis. C.M.Q. contributed to the NMR experiments. G.Y. solved the crystal structure. J.S. and I.V.S. contributed to the interpretation of the results. M.P.F. and T.P. took the lead in writing the manuscript. All authors discussed the results and contributed to the manuscript preparation.

Table 1. Peak assignment of fluorinated model compounds on the basis of DFT calculations and experimental ^{19}F spin-lattice relaxation times (T_1).

Molecule	Assignment	δ_{iso} (ppm) MAS NMR	σ_{iso} (ppm) DFT	δ_{iso} (ppm) DFT	T_1 (s) MAS NMR
2,3-difluorobenzoic acid	2F	-35.8	313.4	-141.6	471.0
	3F	-39.8	314.7	-142.9	487.2
2,4-difluorobenzoic acid	2F	-27.0	278.9	-100.7	352.5
	4F	-22.6	272.5	-118.5	459.3
2,5-difluorobenzoic acid	2F	-60.4	290.3	-118.5	917.5
	5F	-62.9	294.7	-123.0	926.3
7F-L-Tryptophan	F_1	-53.1	308.5	-136.8	212.0
	F_2	-56.4	312.2	-140.4	215.0

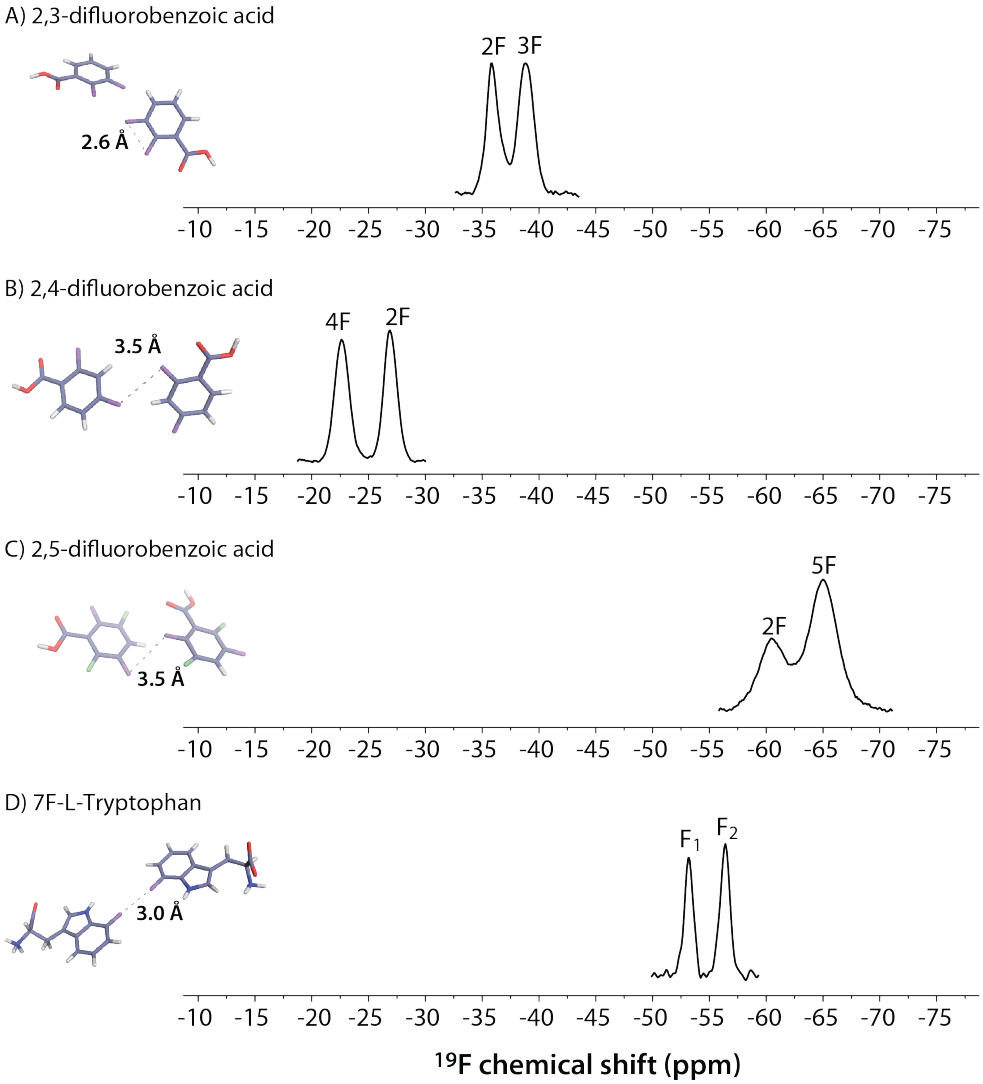

Figure 1. Structures and ^{19}F MAS NMR spectra of several fluorinated aromatic compounds: A) 2,3-difluorobenzoic acid, B) 2,4-difluorobenzoic acid, c) 2,5-difluorobenzoic acid, and d) 7-F-L-Tryptophan. Spectra were recorded at 14.1 T and the MAS frequency was 60 kHz. Resonance assignments are provided above the resonances. In the structures, the shortest interfluorine distance is labeled. Note that for 2,3-difluorobenzoic acid this is the intramolecular interfluorine distance, while for the rest of the compounds the shortest distance is intermolecular.

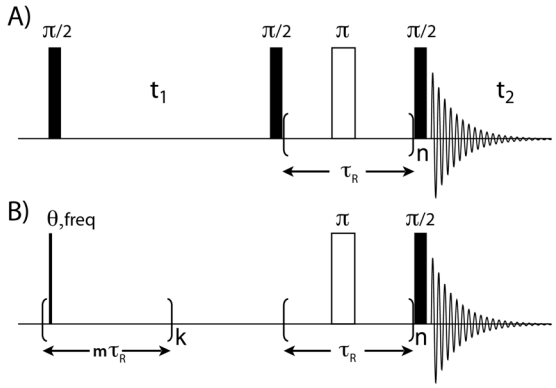

Figure 2. A-B) Pulse sequences used for ^{19}F-^{19}F dipolar recoupling: A) 2D RFDR[23] and B) 1D DANTE-RFDR build-up experiment[24] where 0.1 μs DANTE pulses were used for selective inversion prior to RFDR mixing. The DANTE interpulse delays were set to 1 or 2 rotor periods.

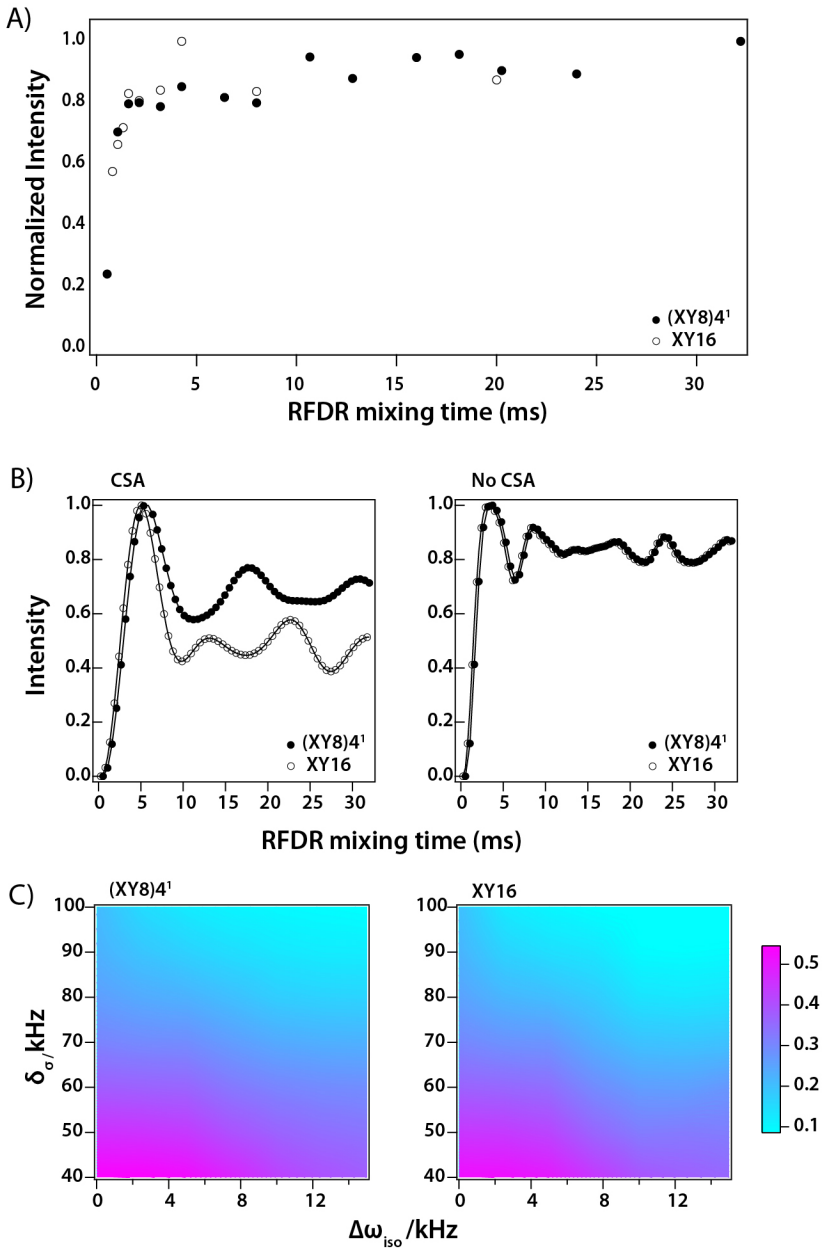

Figure 3. A) Experimental 2D RFDR buildup curve for 7F-L-Trp recorded with both XY16 and (XY8)4^1 phase cycles during RFDR mixing (closed and open circles, respectively). The MAS frequency was 60 kHz. B) Numerical simulations of the ^{19}F longitudinal magnetization exchange in the presence (left) and absence (right) of CSA (δ_σ = 110 ppm; η = 0.5). The length of the π pulse was 0.36 τ_R. The SIMPSON simulation script for generating the XY16 curve is provided in the Supporting Information. C) Dependence of the RFDR signal intensity on the difference in resonance frequency and reduced anisotropy for (XY8)4^1 (left) and XY16 (right) phase cycles. The MAS frequency was 60 kHz and the RFDR mixing time was 6.4 ms. The SIMPSON script for simulating the (XY8)4^1 contour is provided in the Supporting Information. All experimental data as well as the simulations employed a MAS frequency of 60 kHz.

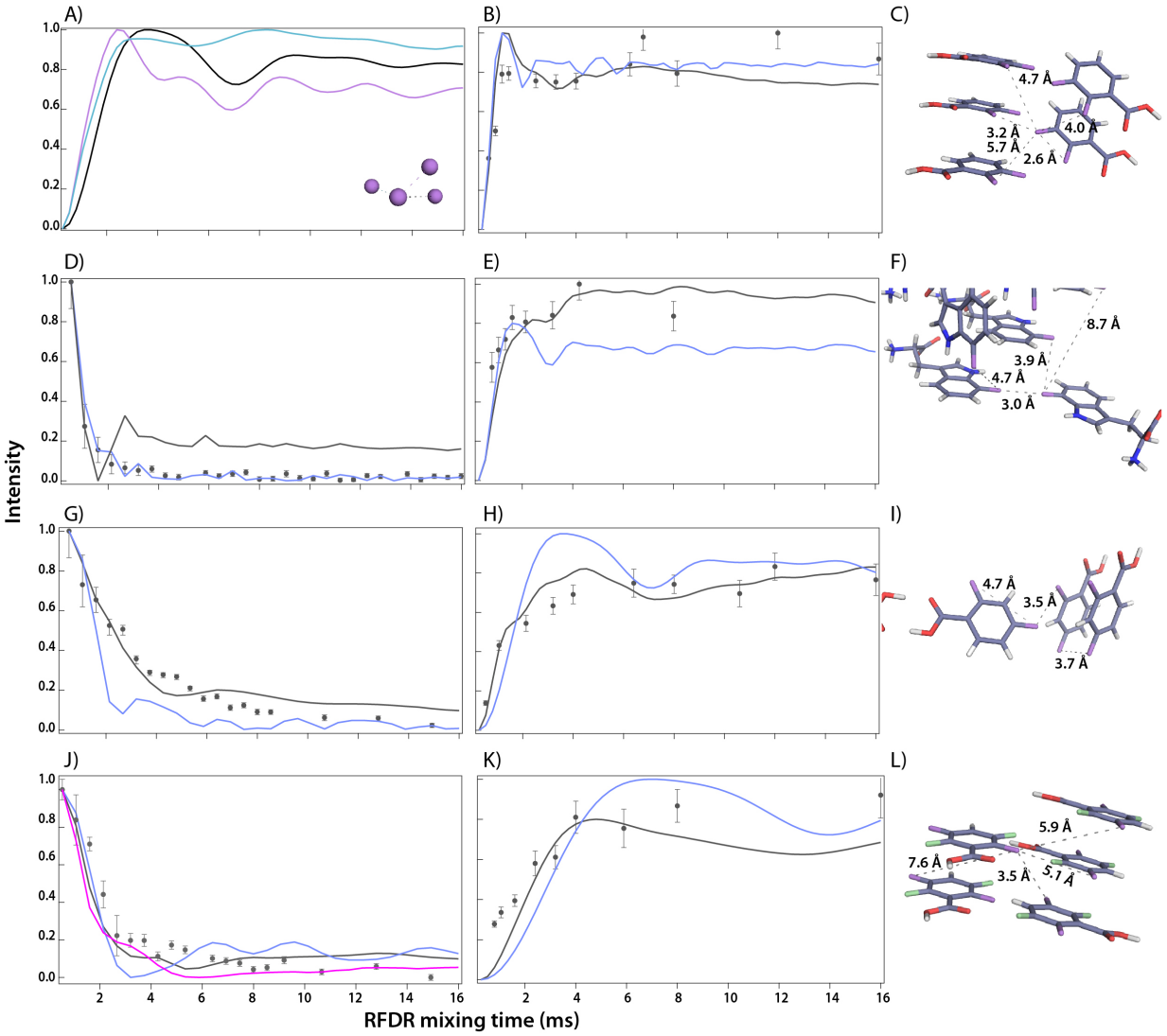

Figure 4. A) Illustration of the effect of multi-spin effects on the RFDR signal buildups. Spectra were recorded at 14.1 T and the MAS frequency was 60 kHz. The buildup curve for a single spin pair (corresponding to the intramolecular distance of 4.2 Å) is shown in blue. The buildup curves for three-spin and four-spin systems are shown in magenta and black, respectively. B) Experimental and simulated (6-spin) 2D RFDR buildup curves for 2,3-dilfuorobenzoic acid. The buildup curve for a single spin pair (corresponding to the intramolecular distance of 2.6 Å) and six spins are shown in blue and black, respectively. The corresponding local environment in the crystal lattice and the relevant distances between the fluorine spins are shown in C). D,E) Experimental and simulated DANTE-RFDR and 2D RFDR buildup curves for 7F-L-Trp; the local environment in the crystal lattice and the relevant distances between the fluorine spins are shown in F). The buildup curve for a single spin pair (corresponding to the intermolecular distance of 3.0 Å) and five spins are shown in blue and black, respectively. G,H) Experimental and simulated DANTE-RFDR and 2D-RFDR for 2,4-dilfuorobenzoic acid; the local environment in the crystal lattice and the coupling network are shown in I). The buildup curve for a single spin pair (corresponding to the intrmolecular distance of 4.7 Å) and five spins are shown in blue and black, respectively. J,K) Experimental and simulated DANTE-RFDR and 2D-RFDR buildup curves for 2,5-dilfuorobenzoic acid. The fluorine atoms are positionally disordered in the crystal with an occupancy of 80% (positional isomer a, fluorine atoms colored purple) and 20% (positional isomer b, fluorine atoms colored light green). The extended network of fluorine spin interactions is shown for the major positional isomer a, with distances labeled. The buildup curve for a single spin pair (corresponding to the intermolecular distance of 5.4 Å) is shown in blue. Simulations taking into account the occupancy of the positional isomers a (80%) and b (20%) in the unit cell are shown in black. The best-fit curve from the simulations of the grid of 3000 five-spin systems is shown in magenta. Details of numerical simulations are discussed in the main text and Supporting Information.

REFERENCES

1. Quinn, C. M.; Polenova, T., Structural biology of supramolecular assemblies by magic-angle spinning NMR spectroscopy. *Q. Rev. Biophys.* **2017,** *50*, e1-e44.
2. Matei, E.; Gronenborn, A. M., ^{19}F paramagnetic relaxation enhancement: a valuable tool for distance measurements in proteins. *Angew. Chem.* **2016,** *55*, 150-154.
3. Wang, M.; Lu, M.; Fritz, M. P.; Quinn, C. M.; Byeon, I. J. L.; Byeon, C. H.; Struppe, J.; Maas, W.; Gronenborn, A. M.; Polenova, T., Fast magic-angle spinning ^{19}F NMR spectroscopy of HIV-1 capsid protein assemblies. *Angew. Chem.* **2018,** *57*, 16375-16379.
4. Campos-Olivas, R.; Aziz, R.; Helms, G. L.; Evans, J. N. S.; Gronenborn, A. M., Placement of ^{19}F into the center of GB1: effects on structure and stability. *FEBS Lett.* **2002,** *517*, 55-60.
5. Crowley, P. B.; Kyne, C.; Monteith, W. B., Simple and inexpensive incorporation of ^{19}F-tryptophan for protein NMR spectroscopy. *Chem. Commun.* **2012,** *48*, 10681-10683.
6. Gakh, Y. G.; Gakh, A. A.; Gronenborn, A. M., Fluorine as an NMR probe for structural studies of chemical and biological systems. *Magn. Reson. Chem.* **2000,** *38*, 551-558.
7. Sharaf, N. G.; Gronenborn, A. M., ^{19}F-Modified Proteins and ^{19}F-Containing Ligands as Tools in Solution NMR Studies of Protein Interactions. In *Isotope Labeling of Biomolecules - Labeling Methods*, Kelman, Z., Ed. Elsevier Academic Press Inc: San Diego, 2015; Vol. 565, pp 67-95.
8. Wang, J.; Sanchez-Rosello, M.; Acena, J. L.; del Pozo, C.; Sorochinsky, A. E.; Fustero, S.; Soloshonok, V. A.; Liu, H., Fluorine in pharmaceutical industry: fluorine-containing drugs introduced to the market in the last decade (2001-2011). *Chem. Rev.* **2014,** *114*, 2432-2506.
9. Lu, M. M.; Wang, M. Z.; Sergeyev, I. V.; Quinn, C. M.; Struppe, J.; Rosay, M.; Maas, W.; Gronenborn, A. M.; Polenova, T., ^{19}F dynamic nuclear polarization at fast magic angle spinning for NMR of HIV-1 capsid protein assemblies. *J. Am. Chem. Soc.* **2019,** *141*, 5681-5691.
10. Roos, M.; Mandala, V. S.; Hong, M., Determination of long-range distances by fast magic-angle-spinning radiofrequency-driven ^{19}F-^{19}F dipolar recoupling NMR. *J. Phys. Chem. B* **2018,** *122*, 9302-9313.
11. Shcherbakov, A. A.; Hong, M., Rapid measurement of long-range distances in proteins by multidimensional ^{13}C-^{19}F REDOR NMR under fast magic-angle spinning. *J. Biomol. NMR* **2018,** *71*, 31-43.
12. Shcherbakov, A. A.; Mandala, V. S.; Hong, M., High-sensitivity detection of nanometer ^{1}H-^{19}F distances for protein structure determination by ^{1}H-detected fast MAS NMR. *J. Phys. Chem. B* **2019,** *123*, 4387-4391.
13. Kozorog, M.; Sani, M.-A.; Separovic, F.; Anderluh, G., Listeriolysin O binding affects cholesterol and phospholipid acyl chain dynamics in fluid cholesterol-rich bilayers. *Chem. Eur. J.* **2018,** *24*, 14220-14225.
14. Graesser, D. T.; Wylie, B. J.; Nieuwkoop, A. J.; Franks, W. T.; Rienstra, C. M., Long-range ^{19}F-^{15}N distance measurements in highly-^{13}C, ^{15}N-enriched solid proteins with ^{19}F-dephased REDOR shift (FRESH) spectroscopy. *Magn. Reson. Chem.* **2007,** *45 Suppl 1*, S129-34.
15. Lu, M. M.; Sarkar, S.; Wang, M. Z.; Kraus, J.; Fritz, M.; Quinn, C. M.; Bai, S.; Holmes, S. T.; Dybowski, C.; Yap, G. P. A., et al., ^{19}F magic angle spinning NMR spectroscopy and density functional theory calculations of fluorosubstituted tryptophans: integrating experiment and theory for accurate determination of chemical shift tensors. *J. Phys. Chem. B* **2018,** *122*, 6148-6155.
16. Lu, X. Y.; Skomski, D.; Thompson, K. C.; McNevin, M. J.; Xu, W.; Su, Y., Three-dimensional NMR spectroscopy of fluorinated pharmaceutical solids under ultrafast magic angle spinning. *Anal. Chem.* **2019,** *91*, 6217-6224.

17. Karlsson, T.; Popham, J. M.; Long, J. R.; Oyler, N.; Drobny, G. P., A study of homonuclear dipolar recoupling pulse sequences in solid-state nuclear magnetic resonance. *J. Am. Chem. Soc.* **2003,** *125*, 7394-7407.
18. Courtney, J. M.; Rienstra, C. M., Efficient dipolar double quantum filtering under magic angle spinning without a ^{1}H decoupling field. *J. Magn. Reson.* **2016,** *269*, 152-156.
19. Hou, G. J.; Yan, S.; Trebosc, J.; Amoureux, J. P.; Polenova, T., Broadband homonuclear correlation spectroscopy driven by combined $R2_n^v$ sequences under fast magic angle spinning for NMR structural analysis of organic and biological solids. *J. Magn. Reson.* **2013,** *232*, 18-30.
20. Hu, B. W.; Lafon, O.; Trebosc, J.; Chen, Q.; Amoureux, J. P., Broad-band homo-nuclear correlations assisted by ^{1}H irradiation for bio-molecules in very high magnetic field at fast and ultra-fast MAS frequencies. *J. Magn. Reson.* **2011,** *212*, 320-329.
21. Weingarth, M.; Bodenhausen, G.; Tekely, P., Broadband carbon-13 correlation spectra of microcrystalline proteins in very high magnetic fields. *J. Am. Chem. Soc.* **2009,** *131*, 13937-13939.
22. Weingarth, M.; Masuda, Y.; Takegoshi, K.; Bodenhausen, G.; Tekely, P., Sensitive ^{13}C-^{13}C correlation spectra of amyloid fibrils at very high spinning frequencies and magnetic fields. *J. Biomol. NMR* **2011,** *50*, 129-136.
23. Bennett, A. E.; Griffin, R. G.; Ok, J. H.; Vega, S., Chemical shift correlation spectroscopy in rotating solids: radio frequency ‐ driven dipolar recoupling and longitudinal exchange. *J. Chem. Phys.* **1992,** *96*, 8624-8627.
24. Gilchrist, M. L.; Monde, K.; Tomita, Y.; Iwashita, T.; Nakanishi, K.; McDermott, A. E., Measurement of interfluorine distances in solids. *J. Magn. Reson.* **2001,** *152*, 1-6.
25. Zhang, R. C.; Nishiyama, Y.; Sun, P. C.; Ramamoorthy, A., Phase cycling schemes for finite-pulse-RFDR MAS solid state NMR experiments. *J. Magn. Reson.* **2015,** *252*, 55-66.
26. Bayro, M. J.; Ramachandran, R.; Caporini, M. A.; Eddy, M. T.; Griffin, R. G., Radio frequency-driven recoupling at high magic-angle spinning frequencies: homonuclear recoupling *sans* heteronuclear decoupling. *J. Chem. Phys.* **2008,** *128*, 052321-1-052321-11.
27. Shen, M.; Hu, B. W.; Lafon, O.; Trebosc, J.; Chen, Q.; Amoureux, J. P., Broadband finite-pulse radio-frequency-driven recoupling (fp-RFDR) with $(XY8)4^{1}$ super-cycling for homo-nuclear correlations in very high magnetic fields at fast and ultra-fast MAS frequencies. *J. Magn. Reson.* **2012,** *223*, 107-119.
28. Ishii, Y., ^{13}C-^{13}C dipolar recoupling under very fast magic angle spinning in solid-state nuclear magnetic resonance: applications to distance measurements, spectral assignments, and high-throughput secondary-structure determination *J. Chem. Phys.* **2001,** *114*, 8473-8483.
29. Bodenhausen, G.; Freeman, R.; Morris, G. A., A simple pulse sequence for selective excitation in Fourier transform NMR. *J. Magn. Reson.* **1976,** *23*, 171-175.
30. Dubey, R.; Pavan, M. S.; Desiraju, G. R., Structural landscape of benzoic acid: using experimental crystal structures of fluorobenzoic acids as a probe. *Chem. Commun.* **2012,** *48*, 9020-9022.
31. *Apex3*, Bruker AXS Inc: Madison, WI, 2015.
32. Sheldrick, G. M., SHELXT - integrated space-group and crystal-structure determination. *Acta Cryst. A* **2015,** *71*, 3-8.
33. Sheldrick, G. M., Crystal structure refinement with SHELXL. *Acta Cryst. C* **2015,** *71*, 3-8.
34. Maurer, T.; Kalbitzer, H. R., Indirect referencing of P-31 and F-19 NMR spectra. *J. Magn. Reson. Ser. B* **1996,** *113*, 177-178.
35. Marion, D.; Wuthrich, K., Application of phase sensitive two-dimensional correlated spectroscopy (COSY) for measurements of ^{1}H-^{1}H spin-spin coupling-constants in proteins. *Biochem. Biophys. Res. Commun.* **1983,** *113*, 967-974.

36. Lee, W.; Tonelli, M.; Markley, J. L., NMRFAM-SPARKY: enhanced software for biomolecular NMR spectroscopy. *Bioinformatics* **2015,** *31*, 1325-1327.
37. Delaglio, F.; Grzesiek, S.; Vuister, G. W.; Zhu, G.; Pfeifer, J.; Bax, A., NMRPIPE - a multidimensional spectral processing system based on unix pipes. *J. Biomol. NMR* **1995,** *6*, 277-293.
38. Frisch, M. J.; Trucks, G. W.; Schlegel, H. B.; Scuseria, G. E.; Robb, M. A.; Cheeseman, J. R.; Scalmani, G.; Barone, V.; Mennucci, B.; Petersson, G. A., et al. *Gaussian 09, Revision B.01*, Wallingford CT, 2009.
39. Marenich, A. V.; Cramer, C. J.; Truhlar, D. G., Universal solvation model based on solute electron density and on a continuum model of the solvent defined by the bulk dielectric constant and atomic surface tensions. *J. Phys. Chem. B* **2009,** *113*, 6378-6396.
40. Zhao, Y.; Truhlar, D. G., The M06 suite of density functionals for main group thermochemistry, thermochemical kinetics, noncovalent interactions, excited states, and transition elements: Two new functionals and systematic testing of four M06-class functionals and 12 other functionals. *Theor. Chem. Acc.* **2008,** *120*, 215-241.
41. Isley, W. C.; Urick, A. K.; Pomerantz, W. C. K.; Cramer, C. J., Prediction of ^{19}F NMR chemical shifts in labeled proteins: computational protocol and case study. *Mol. Pharm.* **2016,** *13*, 2376-2386.
42. Bak, M.; Rasmussen, J. T.; Nielsen, N. C., SIMPSON: a general simulation program for solid-state NMR spectroscopy. *J. Magn. Reson.* **2000,** *147*, 296-330.
43. Zaremba, S. K., Good lattice points, discrepancy, and numerical integration. *Ann. Mat. Pur. Appl.* **1966,** *73*, 293-317.
44. Bak, M.; Nielsen, N. C., REPULSION, a novel approach to efficient powder averaging in solid-state NMR. *J. Magn. Reson.* **1997,** *125*, 132-139.
45. Saunders, C.; Khaled, M. B.; Weaver, J. D.; Tantillo, D. J., Prediction of ^{19}F NMR chemical shifts for fluorinated aromatic compounds. *J. Org. Chem.* **2018,** *83*, 3220-3225.
46. Boeszoermenyi, A.; Chhabra, S.; Dubey, A.; Radeva, D. L.; Burdzhiev, N. T.; Chanev, C. D.; Petrov, O. I.; Gelev, V. M.; Zhang, M.; Anklin, C., et al., Aromatic ^{19}F-^{13}C TROSY: a background-free approach to probe biomolecular structure, function, and dynamics. *Nat. Methods* **2019,** *16*, 333-340.
47. Boender, G. J.; Vega, S., Phase sensitive detection of 2D homonuclear correlation spectra in MAS NMR. *J. Magn. Reson.* **1998,** *133*, 281-285.
48. Levitt, M. H.; Raleigh, D. P.; Creuzet, F.; Griffin, R. G., Theory and simulations of homonuclear spin pair systems in rotating solids. *J. Chem. Phys.* **1990,** *92*, 6347-6364.
49. Bayro, M. J.; Huber, M.; Ramachandran, R.; Davenport, T. C.; Meier, B. H.; Ernst, M.; Griffin, R. G., Dipolar truncation in magic-angle spinning NMR recoupling experiments. *J. Chem. Phys.* **2009,** *130*, 8.
50. Martineau, C.; Senker, J.; Taulelle, F., NMR crystallography. *Annu. Rep. NMR Spectrosc.* **2014,** *82*, 1-57.
51. Monde, K.; Tomita, Y.; Gilchrist, M. L.; McDermott, A. E.; Nakanishi, K., Design and preparation of polyphenyl distance markers for solid-state ^{19}F NMR. *Isr. J. Chem.* **2000,** *40*, 301-306.

TOC Graphic

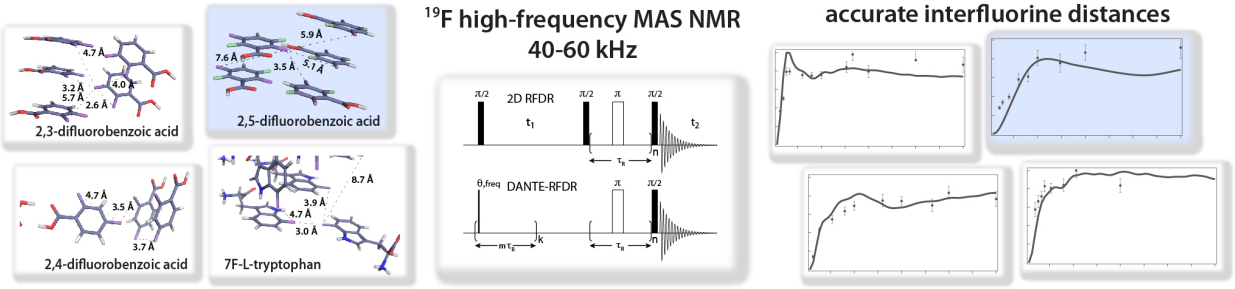
4.7 Å
3.2 Å
4.0 Å
5.7 Å
2.6 Å
2,3-difluorobenzoic acid
5.9 Å
7.6 Å
3.5 Å
5.7 Å
2,5-difluorobenzoic acid
4.7 Å
3.5 Å
3.7 Å
2,4-difluorobenzoic acid
8.7 Å
3.9 Å
4.7 Å
3.0 Å
7F-L-tryptophan
19F high-frequency MAS NMR
40-60 kHz
2D RFDR
DANTE-RFDR
accurate interfluorine distances